

CMB COLD SPOT IN THE PLANCK LIGHT

M. FARHANG¹, S. M. S. MOVAHED^{1,2,3}

¹Department of Physics, Shahid Beheshti University, Velenjak, Tehran 19839, Iran

²Ibn-Sina Multidisciplinary Laboratory, Department of Physics, Shahid Beheshti University, Velenjak, Tehran 19839, Iran

³School of Physics, Institute for Research in Fundamental Sciences (IPM), P. O. Box 19395-5531, Tehran, Iran

Draft version December 21, 2024

ABSTRACT

The Cold Spot is a statistically significant anomaly in the Cosmic Microwave Background (CMB) sky. In this work, we assess whether a huge void or a cosmic texture could have produced such an anomaly through searching for their gravitational redshift (Rees-Sciama effect) and lensing signatures on the *Planck* CMB sky. In the flat sky approximation, we find the amplitudes for the corresponding templates for both candidates consistent with zero, leaving little room, according to *Planck*, for those structures as the main source of the Cold Spot anomaly.

1. INTRODUCTION

The Cold Spot in the Cosmic Microwave Background (CMB) map is an unusually cold and large region located at $(\ell = 207.8^\circ, b = -56.3^\circ)$ and is among the most significant CMB anomalies. It was first detected in the WMAP data (Vielva et al. 2004; Cruz et al. 2005, 2006) and subsequently confirmed by Planck observations (Planck Collaboration et al. 2016). Figure 1 illustrates the Planck CMB temperature anisotropies with the cold spot (hereafter, CS) patch enlarged. The chances that Gaussian and isotropic initial conditions have led to such a large and relatively cold region are low (Cruz et al. 2005, 2006, 2007). Therefore, there have been speculations of the CS being produced by secondary sources of anisotropy such as a supervoid or a cosmic texture. Inoue & Silk (2007) showed that a huge under-dense region with density contrast $\delta \sim -0.3$ and the comoving radius $R \sim 200h^{-1}\text{Mpc}$ located at $z \approx 1$ could lead to such a pattern of anisotropy. However, both Λ CDM-based simulations (Colberg et al. 2005; Platen et al. 2008) and observational evidence (Patiri et al. 2006; Hoyle & Vogeley 2004; Mackenzie et al. 2017) are against the existence of such a super-void at that redshift. A more probable alternative is a cosmic texture causing a CS on the CMB sky through interactions with the photons passing nearby (Cruz et al. 2007, 2008).

These large scale structures gravitationally interact with CMB photons passing through or nearby them on their way to reach us and lead to their gravitational redshift and lensing. The amplitudes of these imprints can be simultaneously measured. If consistent, these measurements would imply the viability of the assumption used in the template construction. Their inconsistency, on the other hand, may call for a different parameterization of the templates or different parameter values, or even more severely, challenge the existence of the structure and its role in generating the CS.

In this work, we are interested in analyzing the traces such structures, if existing, would leave on the microwave sky as seen by the Planck data and do not intend to assess the feasibility of their formation. The rest of this paper is

organized as follows. In Section 2, we introduce two well-motivated candidates, a huge void and a cosmic texture, used in this work as possible sources of the CS and their imprints on CMB photons. The mathematical framework for the analysis of these imprints is explained in Section 3, and the results are presented in Section 4. We conclude in Section 5. Whenever needed, the standard Λ CDM cosmology, consistent with the Planck 2018 data (Planck Collaboration et al. 2018), is assumed throughout.

2. CANDIDATES

In this section, we introduce two physically motivated candidates as possible origins of the CMB CS, i.e., a cosmic texture (Section 2.1) and a huge void (Section 2.2). We discuss the gravitational redshift and lensing of CMB photons as they pass through or close to these intervening structures. Given the small size of the sky patch we are interested in, we work in the flat sky limit.

2.1. Cosmic Texture

Among the most plausible explanations for the observed CMB CS is a collapsing cosmic texture, first proposed by Cruz et al. (2007). Cosmic textures are a type of topological defect possibly formed in phase transitions at early times, associated with symmetry breaking of certain models of high-energy physics (Turok 1989). The photons passing through the non-static gravitational potential of a collapsing texture would experience gravitational redshift and therefore a decrease in their temperature. Such temperature anisotropies produced at small angular scales are approximated by (Pen et al. 1994):

$$\delta T_{\text{rs}}(r) = \epsilon \frac{1}{\sqrt{1 + 4 \frac{r^2}{R_{\text{T}}^2}}}. \quad (1)$$

here $\delta T \equiv \Delta T/T$ and r represents the angular separation (in radian) of the direction of the observation to the CS center. The R_{T} is the characteristic angular scale of the texture, determined by the dynamics of the Universe, as well as the redshift of the texture z_{T} . The subscript "rs" corresponds to Rees-Sciama effect (Rees & Sciama 1968). The ϵ in Eq. (1) is associated with the

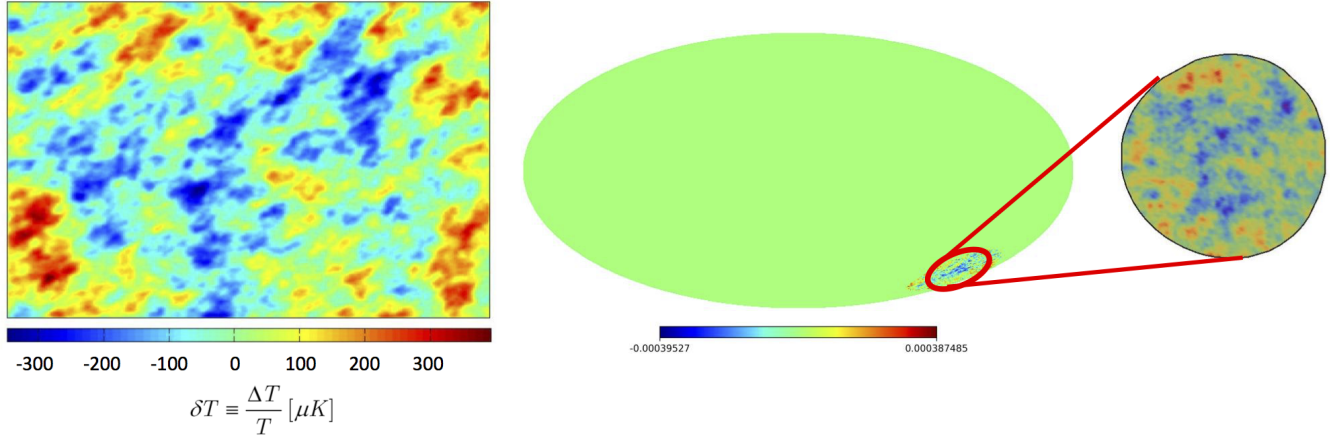


FIG. 1.— Left panel: The Cold Spot patch as seen by *Planck*. Right panel: The position of the Cold Spot anomaly in the southern hemisphere of the microwave sky, with the Cold Spot patch enlarged.

energy scale, ψ_0 , of the symmetry breaking phase transition through $\epsilon = 8\pi^2 G\psi_0^2$. It should be noted that the approximate profile of Eq. (1) is only valid for temperature anisotropies up to $r \approx R_T$. It can be extended to larger separations assuming the continuity of the profile and its first derivative at R_T .

In addition to generating anisotropies in the microwave sky by gravitational redshift, the texture potential also acts as a converging lens and bends the trajectories of the photons passing through it. Accordingly, the lensed temperature field, $\delta\tilde{T}$, for small radial deflection angle is expressed as

$$\delta\tilde{T}(r) = \delta T(r + \alpha(r)) \simeq \delta T(r) + \delta T_{\text{lens}}(r), \quad (2)$$

where δT is the unlensed map, $\delta T_{\text{lens}} \equiv \alpha(r)\partial\delta T(r)/\partial r$ and $\alpha(r)$ is the template for the lensing deflection angle. For the cosmic texture, this template is modeled by (Durrer et al. 1992; Das & Spergel 2009)

$$\alpha_T(r) = A_T \frac{r}{\sqrt{1 + 4\frac{r^2}{R_T^2}}}. \quad (3)$$

here $A_T \equiv \frac{2\sqrt{2}\epsilon}{R_T} \frac{D_{\text{LS}}}{D_S}$, with D_S and D_{LS} representing the comoving distances of the source (i.e., the last scattering surface) to the observer and to the lens, respectively.

We follow the template fitting of earlier works based on WMAP data (Cruz et al. 2007) to adopt $\epsilon = 4 \times 10^{-5}$ and $R_T = 5^\circ$. This places the texture at redshift $z_T \sim 6$ and gives $A_T = 5.10 \times 10^{-4}$.

2.2. Huge Void

Expanding local void can produce gravitational redshift and thus temperature decrements in the CMB photons passing through them, the so-called Rees-Sciama effect (Rees & Sciama 1968). Inoue & Silk (2006, 2007) proposed that the observed CMB CS can be produced by such a void. In particular, they showed that a compensating spherically symmetric void (i.e., one surrounded by a thin shell of matter that contains all the matter supposed to be in the void) with comoving radius $R_V \sim 300h^{-1}\text{Mpc}$ and density contrast $\delta_V \sim -0.3$, located at redshift $z_V < 1$, can explain the CS in the mi-

crowave sky. A completely empty void, i.e., with $\delta_V \sim -1$, would require a smaller radius $R_V \sim 120h^{-1}\text{Mpc}$ to agree with observations (Rudnick et al. 2007). However, simulations suggest typical void sizes of $\sim 10h^{-1}$ (with $\delta_V \sim -0.8$), rendering such huge void extremely unlikely to find (Patiri et al. 2006; Hoyle & Vogeley 2004; Colberg et al. 2005; Platen et al. 2008; Mackenzie et al. 2017). As already stated, we only assess the detectability of the gravitational traces of such a super void on the CMB temperature anisotropies as seen by *Planck* and do not address the likeliness of its existence.

Martinez-Gonzalez & Sanz (1990) use approximations to Einstein field equations for the linear non-static potential generated by non-linear density fluctuations to study the propagation of light and derive relatively simple expressions for the induced anisotropies in the CMB sky. Assuming an empty spherical and compensated void placed at redshift z as the structure, with a length scale much smaller than the Hubble radius D_H , they find the following approximation for the generated anisotropy by the gravitational redshift of photons¹,

$$\delta T_{\text{rs}}(r) \approx \frac{16}{3} \left(\frac{R_V}{1 - d \cos r} \right)^3 \sqrt{1 - \frac{d^2 \sin^2 r}{R_V^2}} \left(\frac{9}{2} \gamma - 4 + \frac{d^2 \sin^2 r}{R_V^2} \right), \quad (4)$$

where $R_V \propto t^\gamma$ with $\gamma \equiv E(z) \int_z^\infty (1+z')^{-1} E(z')^{-1} dz'$ describing the propagation of the shell. We also have $E(z) \equiv H(z)/H_0$ and $H(z)$ is the Hubble parameter and d represents our comoving distance to the center of the shell D_L in units where the horizon size is unity, i.e., $d \equiv D_L/D_H = \int_0^z E(z')^{-1} dz' / \int_0^\infty E(z')^{-1} dz'$. As in Eq. (1), r represents the angular distance between the direction of the observation and the center of the structure.

Besides the gravitational redshift, the photons that pass through the void also experience gravitational lensing. With the above assumptions for the void, the

¹ The result in Martinez-Gonzalez & Sanz (1990) is for an Einstein-de Sitter Universe, which extends to the above Λ CDM universe with straightforward replacements.

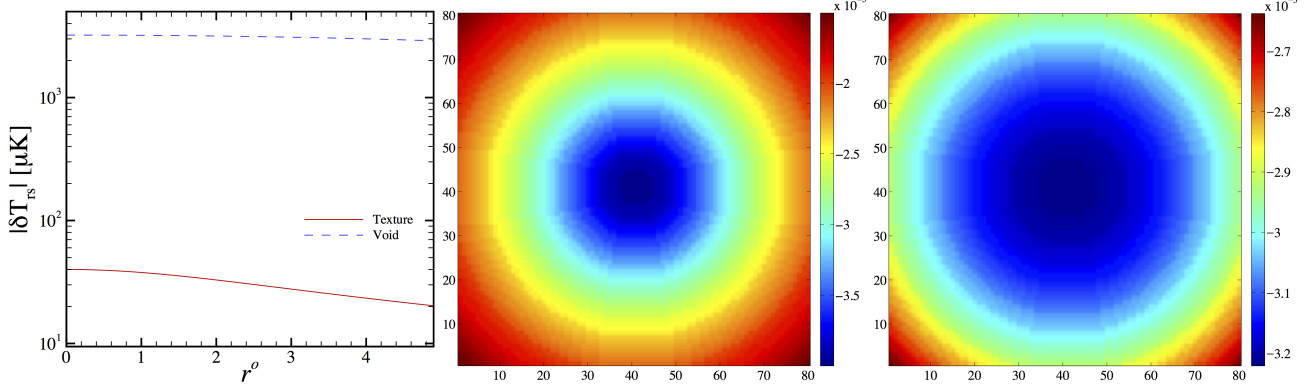


FIG. 2.— Left: The radial profile of temperature anisotropies due to gravitational redshift of a cosmic texture (red solid line) and a huge void (blue dashed line). Middle and right: Patches of temperature anisotropy maps generated by the gravitational redshift of a cosmic texture and a void respectively. The patches have 80^2 pixels and sides of 9.3° .

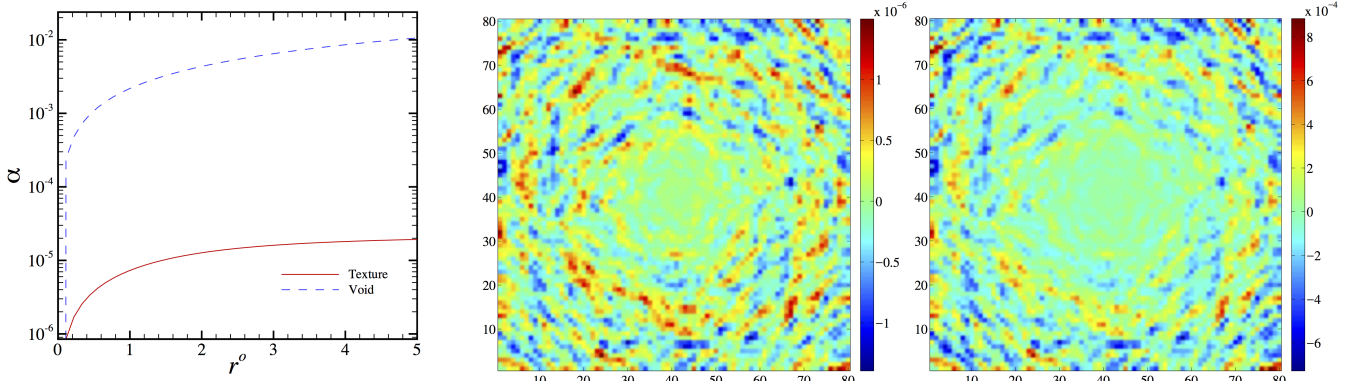


FIG. 3.— Similar to Fig. 2, but with the radial profile and anisotropies corresponding to the gravitational lensing of a cosmic texture (middle) and a void (right).

deflection angle is shown to be well-approximated by (Martinez-Gonzalez & Sanz 1990):

$$\alpha(r) \approx 8dR_V \sin r(1 - R_V^{-2}d^2 \sin^2 r)^{1/2}. \quad (5)$$

In this work, we assume an empty void ($\delta_V \sim -1$) with $R_V = 4.42^\circ$, located at $z_V = 0.8$. The deflection angle is maximum at $r_{\max} \sim 15.65^\circ$.

Figures 2 and 3 illustrate the redshift and deflection angle templates for the models discussed above. The left panels present the radial profiles for the cosmic texture (red solid curve) and the compensated void (blue dashed curve) while the middle and right panels show the induced CMB anisotropies produced by these two structures respectively. The square patches in the middle and right panels are of side 9.3° with 6400 pixels.

3. ANALYSIS

In the previous section, we discussed the theoretical framework for the contribution to CMB anisotropies from the gravitational effects of a cosmic texture and a huge compensated void. We now explain our analysis method with the aim to investigate the detectability (and consistency) of the traces of these structures by the *Planck* data. The main data set consists of a disk of radius $R = 6^\circ$, centered at the center of the CS with galac-

tic coordinates $(\ell = 207.8^\circ, b = -56.3^\circ)$, cut from the *Planck* temperature map² (see Figure 1 for more details). For comparison, we also use several non-overlapping null patches with the same radius centered at various points on the sphere. The results presented here are with the Healpix³ resolution characterized by $N_{\text{side}} = 512$, corresponding to the pixel size of $\approx 7'$. For a joint analysis of the gravitational redshift and lensing trace of the two candidates, assume that the observed temperature anisotropy of the patch can be modeled as:

$$\delta T_{\text{obs}} = \delta T_{\text{pri}} + \mathcal{A}_{\text{rs}} \delta T_{\text{rs}} + \mathcal{A}_{\text{lens}} \delta T_{\text{lens}} + n \quad (6)$$

where $\delta T_{\text{obs}} \equiv \Delta T/T|_{\text{observed}}$ and $\delta T_{\text{pri}} \equiv \Delta T/T|_{\text{primordial}}$ represent the observed and primordial CMB anisotropies while δT_{rs} and δT_{lens} are the anisotropies due to the gravitational redshift and lensing of photons from the assumed templates. The instrumental noise is represented by n . The template δT_{rs} represents the gravitational redshift produced by some decaying potential, here, due to a collapsing texture, Eq. (1) or an expanding void, Eq. (4). The δT_{lens} describes the fluctuations due to the lensing of the CMB photons (Eq. 2) by the same source, characterized by

² <https://pla.esac.esa.int/#home>

³ <https://healpix.sourceforge.io>

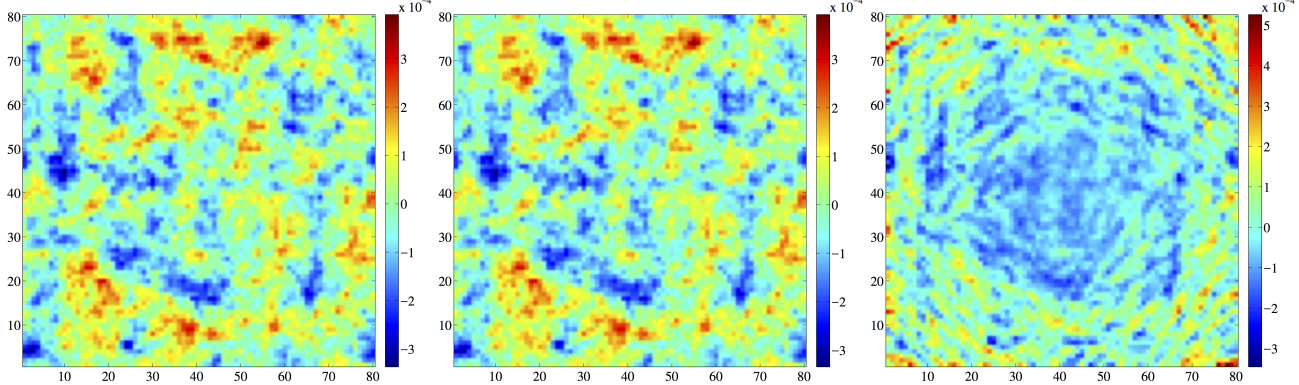


FIG. 4.— Left: The simulated primary CMB anisotropy map (δT_{pri}). Middle: The primary CMB map (as the left panel) with the gravitational effects of a cosmic texture superposed. In other words, this map is the linear combination of the primary CMB map and the middle plots of Fig. 2 and 3. Right: Similar to the middle panel, but for a huge void. See Eq 6 with the amplitudes \mathcal{A}_{rs} and $\mathcal{A}_{\text{lens}}$ set to unity. No instrumental noise is included in these maps.

the deflection angle $\alpha(r)$, Eq. (3) or Eq. (5). Figure 4 compares the simulated primordial anisotropies (left) with maps where the effect of a cosmic texture (middle) or a void (right) is also included according to Eq. 6 with $\mathcal{A}_{\text{rs}} = \mathcal{A}_{\text{lens}} = 1$ and in the absence of any instrumental noise.

The corresponding amplitudes for the templates, \mathcal{A}_{rs} and $\mathcal{A}_{\text{lens}}$, are free parameters to be simultaneously estimated from the data, and are expected to agree if our assumed scenario of the source of the CS makes a consistent picture. Disagreements would then hint to possible inconsistencies in the redshift and lensing templates, improper parameter values fixed *a priori* for template construction, or even, may challenge the plausibility of the model. Within this framework, the likelihood of data, \mathcal{L} , given the CS parameter pair $(\mathcal{A}_{\text{lens}}, \mathcal{A}_{\text{rs}})$ can be expressed through

$$-2 \ln \mathcal{L}(g | \mathcal{A}_{\text{lens}}, \mathcal{A}_{\text{rs}}) = g^T \mathbf{C}^{-1} g + \text{constant} \quad (7)$$

where $g = g(\mathcal{A}_{\text{lens}}, \mathcal{A}_{\text{rs}}) = \delta T_{\text{obs}} - (\mathcal{A}_{\text{rs}} \delta T_{\text{rs}} + \mathcal{A}_{\text{lens}} \delta T_{\text{lens}})$ is the Gaussian signal left when the two CS contributions, $\mathcal{A}_{\text{rs}} \delta T_{\text{rs}} + \mathcal{A}_{\text{lens}} \delta T_{\text{lens}}$, are properly subtracted from the observed data, δT_{obs} . We have made the simplifying assumption that the background primordial signal as well as the instrumental noise can be considered Gaussian. We construct the theoretically expected pixel-pixel covariance matrix for this Gaussian part, $\mathbf{C}_{pp'} \equiv \langle g_p g_{p'}^T \rangle$, from the full sky (except for the mask) *Planck Smica* temperature map. More specifically, we build the correlation function, $C(r)$, where r is the angular separation of any pixel pair on the sphere, and use $C(r)$ to construct the \mathbf{C} matrix for the desired patch. Assuming uniform prior on the parameters, the best-fit values of the parameter pair maximize the likelihood:

$$\frac{\partial \mathcal{L}}{\partial \mathcal{A}_{\text{rs}}} = 0, \quad \frac{\partial \mathcal{L}}{\partial \mathcal{A}_{\text{lens}}} = 0 \quad (8)$$

yielding:

$$\begin{aligned} \mathcal{A}_{\text{rs}} &= \gamma (\delta T_{\text{lens}}^\dagger \mathbf{C}^{-1} \delta T_{\text{lens}}) (\delta T_{\text{rs}}^\dagger \mathbf{C}^{-1} \delta T_{\text{obs}}) \\ &\quad - (\delta T_{\text{rs}}^\dagger \mathbf{C}^{-1} \delta T_{\text{lens}}) (\delta T_{\text{lens}}^\dagger \mathbf{C}^{-1} \delta T_{\text{obs}}) \end{aligned} \quad (9)$$

$$\begin{aligned} \mathcal{A}_{\text{lens}} &= \gamma (\delta T_{\text{rs}}^\dagger \mathbf{C}^{-1} \delta T_{\text{rs}}) (\delta T_{\text{lens}}^\dagger \mathbf{C}^{-1} \delta T_{\text{obs}}) \\ &\quad - (\delta T_{\text{lens}}^\dagger \mathbf{C}^{-1} \delta T_{\text{rs}}) (\delta T_{\text{rs}}^\dagger \mathbf{C}^{-1} \delta T_{\text{obs}}) \end{aligned} \quad (10)$$

where

$$\begin{aligned} \gamma^{-1} &\equiv (\delta T_{\text{rs}}^\dagger \mathbf{C}^{-1} \delta T_{\text{rs}}) (\delta T_{\text{lens}}^\dagger \mathbf{C}^{-1} \delta T_{\text{lens}}) \\ &\quad - (\delta T_{\text{rs}}^\dagger \mathbf{C}^{-1} \delta T_{\text{lens}}) (\delta T_{\text{lens}}^\dagger \mathbf{C}^{-1} \delta T_{\text{rs}}). \end{aligned} \quad (11)$$

We also perform the analysis on N null patches where one expects amplitudes consistent with zero. We then use the variance of the \mathcal{A}_{rs} and $\mathcal{A}_{\text{lens}}$ of these null patches:

$$\sigma_{\diamond, i}^2 = \frac{\sum_i (\mathcal{A}_{\diamond, i} - \bar{\mathcal{A}}_{\diamond})^2}{N - 1}, \quad (12)$$

to assess the statistical significance of the measured \mathcal{A}_{rs} and $\mathcal{A}_{\text{lens}}$ for the Cold Spot patch. Here \diamond stands for rs or lens and the over-bar indicates the averaged value of the measurements.

One could alternatively use the width of the likelihood surface, i.e., the square root of the diagonals of the Fisher inverse, to get an estimate of the parameter measurement error. This yields a reliable estimate of the uncertainties if the posterior probability distribution is close to Gaussian. Otherwise, the errors are smaller than the true uncertainties. In our analysis, we found that the dispersion in the estimated signal amplitudes for the null patches is larger than the Fisher-based errors. Therefore, we chose to be conservative by reporting the results of the former method as a measure of the parameter uncertainty.

4. RESULTS

We followed the method as detailed in the previous section, and used $N = 30$ null patches to get an estimate for the parameter errors. Table 4 summarizes the results at $N_{\text{side}} = 512$. However, we found that for both candidates used in this work, the observed amplitudes are consistent with zero. This means these two templates are not recognized by the *Planck* data as a viable origin for

TABLE 1

THE MEASURED AMPLITUDE OF THE LENSING AND GRAVITATIONAL REDSHIFT TEMPLATES OF A HUGE VOID AND A COSMIC TEXTURE FROM THE PLANCK TEMPERATURE SMICA MAP(2018).

texture	void
$\mathcal{A}_{\text{rs}} = -1.8 \pm 2.5$	$\mathcal{A}_{\text{rs}} = 0.04 \pm 0.10$
$\mathcal{A}_{\text{lens}} = -0.6 \pm 0.6$	$\mathcal{A}_{\text{lens}} = 0.00 \pm 0.02$

the CS. Repeating the analysis at $N_{\text{side}} = 256$ did not change our conclusion.

Improving the theoretical covariance matrix \mathbf{C} is expected to improve the results. For this purpose we estimated \mathbf{C} from 1000 *Planck* 2018 Full Focal Plane (FFP10) simulations as well as the *Planck* 2018 end-to-end simulations where the noise properties of *Planck* maps are taken care of with higher accuracy^{4,5}. However, we found that with these two covariance matrices the measured template amplitudes for some null patches were not consistent with zero. We had checked that the parameter measurement pipeline was unbiased by testing it against simulations of null patches as well as patches including simulations of the CS and found the measured amplitudes for the templates were well consistent with the fiducial values. This analysis could imply that when it comes to detecting delicate signals in the search for anomalies, the theoretical covariance matrix \mathbf{C} from FFP10 and end-to-end simulations may require improvement to properly and thoroughly represent the true observed *Planck* CMB sky. The bias in the simulated maps compared to the true sky was also established in [Akrami et al. \(2018\)](#).

5. SUMMARY AND DISCUSSION

In this work we addressed the possibility of the CMB Cold Spot being produced by a cosmic texture or a huge void. The goal was to search for the signatures of the physical source of the CS on CMB temperature anisotropies, as seen by *Planck*, in the form of gravitational redshift, parameterized by the amplitude \mathcal{A}_{rs} of an assumed template, and a lensing signal with an amplitude $\mathcal{A}_{\text{lens}}$. In the case of a detection (i.e., nonzero amplitudes for the templates), proper comparison of the amplitudes would shed light on the self-consistency of the model. One could even consider exploiting the information in the measured amplitudes to constrain the various physical parameters characterizing the candidate templates. However, we found that the observed amplitudes of the redshift and lensing signals for the assumed void and texture templates are consistent with zero. We also obtained the results based on the covariance matrix from the *Planck* FFP10 simulations to be biased, implying that the simulations may not be fair representatives of the true *Planck* CMB data with the desired accuracy required in this work. We therefore conclude that in the light of the *Planck* data, neither a huge void nor a cosmic texture is recognized as a possible physical source for the CMB CS. Improvement of the measurements and uncertainty reduction could be reached through more precise characterization of the covariance matrix, e.g., by producing more accurate realizations of the *Planck* sky.

Acknowledgement The numerical simulations of this work were carried out on Sunnyvale at the computing cluster of the Canadian Institute for Theoretical Astrophysics (CITA), University of Toronto.

REFERENCES

Akrami, Y., et al. 2018
 Colberg, J. M., Sheth, R. K., Diaferio, A., Gao, L., & Yoshida, N. 2005, MNRAS, 360, 216
 Cruz, M., Martínez-González, E., Vielva, P., & Cayón, L. 2005, MNRAS, 356, 29
 Cruz, M., Martínez-González, E., Vielva, P., Diego, J. M., Hobson, M., & Turok, N. 2008, MNRAS, 390, 913
 Cruz, M., Tucci, M., Martínez-González, E., & Vielva, P. 2006, MNRAS, 369, 57
 Cruz, M., Turok, N., Vielva, P., Martínez-González, E., & Hobson, M. 2007, Science, 318, 1612
 Das, S., & Spergel, D. N. 2009, Phys. Rev. D, 79, 043007
 Durrer, R., Heusler, M., Jetzer, P., & Straumann, N. 1992, Nuclear Physics B, 368, 527
 Hoyle, F., & Vogeley, M. S. 2004, ApJ, 607, 751
 Inoue, K. T., & Silk, J. 2006, ApJ, 648, 23
 —. 2007, ApJ, 664, 650
 Mackenzie, R., Shanks, T., Bremer, M. N., Cai, Y.-C., Gunawardhana, M. L. P., Kovács, A., Norberg, P., & Szapudi, I. 2017, MNRAS, 470, 2328
 Martinez-Gonzalez, E., & Sanz, J. L. 1990, MNRAS, 247, 473
 Patiri, S. G., Betancort-Rijo, J. E., Prada, F., Klypin, A., & Gottlöber, S. 2006, MNRAS, 369, 335
 Pen, U.-L., Spergel, D. N., & Turok, N. 1994, Phys. Rev. D, 49, 692
 Planck Collaboration et al. 2016, A&A, 594, A16
 —. 2018, ArXiv e-prints
 Platen, E., van de Weygaert, R., & Jones, B. J. T. 2008, MNRAS, 387, 128
 Rees, M. J., & Sciama, D. W. 1968, Nature, 217, 511
 Rudnick, L., Brown, S., & Williams, L. R. 2007, ApJ, 671, 40
 Turok, N. 1989, Physical Review Letters, 63, 2625
 Vielva, P., Martínez-González, E., Barreiro, R. B., Sanz, J. L., & Cayón, L. 2004, ApJ, 609, 22

⁴ https://wiki.cosmos.esa.int/planck-legacy-archive/index.php/Simulation_data

⁵ <https://pla.esac.esa.int/#maps>